Accumulation and spatial distribution of CO2 in the astronaut's crew quarters on the International Space Station

M.R. Georgescu, Amina Meslem, I. Nastase

Accumulation and spatial distribution of CO_2 in the astronaut's crew quarters on the International Space Station

Corresponding author: Matei Razvan GEORGESCU[1,2*]

matei.georgescu@univ-rennes1.fr

mateirazvangeorgescu@gmail.com

Phone: +40724818295

Fax number: +40212420781

Postal address: 66 Pache Protopopescu boulevard, 021414

Amina MESLEM[1]

amina.meslem@univ-rennes1.fr

Ilinca NASTASE[2]

ilinca.nastase@utcb.ro

[1]LGCGM, University of Rennes, 3 Rue du Clos Courtel, BP 90422; 35704 Rennes CEDEX 7, France

[2]CAMBI Research Center, Technical University of Civil Engineering of Bucharest, 66 Pache Protopopescu boulevard, Postal code: 021414, Bucharest, Romania

Abstract

In poorly ventilated confined spaces, assessing the accumulation of CO_2 in the breathing zone (BZ) is important evaluating human safety. The current study presents an experimental and numerical investigation of the CO_2 generation rate and spatial distribution in the crew quarters (CQ) of the International Space Station. In microgravity, density-difference based airflow is nonexistent, and CO_2 accumulates around the astronaut's head if the BZ is poorly or not at all ventilated. The aim is to study the breath's influence on CO_2 spatial distribution in order to circumscribe the region that needs to be ventilated in the CQ. An experimental setup was used to measure the CO_2 generation rate of several test subjects on Earth in a non-ventilated full-scale model of the CQ. The experimental CO_2 results were used to validate CFD simulations of the CQ with gravity, with a human model inside featuring a full respiratory cycle. The validated CFD model was then used without gravity for a CO_2 accumulation study. The respiratory cycle was analyzed in order to propose a rigorous definition of the BZ based on a frequency analysis of the breath. Results show that CO_2 concentrations in the identified BZ are greater in the absence of gravity compared to a similar situation with gravity. It is believed that the ventilation system presently in place in the CQ does not effectively ventilate this strategic area, therefore a personalized ventilation type solution should be studied in the future.

Keywords: ISS ventilation, CO_2 accumulation in microgravity, Human breathing simulation, Breathing zone definition.

1. Introduction

The present study is part of a larger investigation concerning the evaluation of the internal environment on the International Space Station (ISS) crew quarters (CQ), where the astronauts sleep. The ISS internal environment has no supply of fresh air. The existing air is reconditioned, CO_2 is scrubbed and oxygen is regenerated by the Environmental Control and Life Support System [1,2]. In microgravity, without ventilation, exhaled CO_2 forms pockets due to the lack of natural convective flows. This problem is aggravated when the astronauts spend long periods of time in confined spaces, like the CQ. Despite the removal of CO_2 from the atmosphere, there have been reports of astronauts suffering from carbon dioxide intoxication after sleeping in the CQ [3–7]. This suggests that CO_2 accumulates in the CQ at a faster rate than the CO_2 scrubber is able to handle. The CO_2 accumulation and its spatial distribution in a confined space are the primary subjects of this paper, tailored to the CQ aboard the ISS but with potential applications for air quality control in other environments.

Standards for the built environment [8] specify that the CO_2 concentration should be between 400 and 1000 ppm over the outdoor level. For reference, at sea level the CO_2 concentration is around 400 ppm. Aboard the ISS, minimum ambient CO_2 concentrations are approximately 3000 ppm, but can reach values greater than 6500 ppm [9]. The mean concentration is not reduced below 3000 ppm because the energy supply is limited. Studies to determine an acceptable upper limit which prevents CO_2 intoxication [9,10] found that variable levels of tolerance to high CO_2 concentrations were developed by the astronauts. Recommendations were to keep the upper limit as low as possible for safety concerns. Identifying and ventilating the above-mentioned CO_2 pockets would be a good compromise.

Studies [11–16] show the importance of on-board ventilation and CO_2 control in the CQ. Extensive use of CFD was made for studying the ventilation in the ISS corridor adjacent to the CQ [12–16] in microgravity. Numerical investigations of the CO_2 accumulation in an older model of the CQ, during fan-failure were performed [8]. A human model generated CO_2 in the virtual CQ, exhaling a constant flow through the nose, calibrated after an astronaut's daily CO_2 generation rate. Important accumulations were found near the chest and mouth of the human model. The constant flow approach is correct in regards to the global mass balance of CO_2 in the CQ, but it does not consider the dynamics of the breathing process which might, influence the local distribution of CO_2 in the vicinity of the astronaut's head where the air is immediately inhaled by the astronaut, causing self-contamination. For ventilation strategies aimed at reducing CO_2 concentrations, information is required regarding CO_2 accumulation in the case of a realistic breathing cycle. To the author's best knowledge, no measurements exist of CO_2 accumulation in the CQ on the ISS.

Mazumdar and Chen [17] and Zhang and Chen [18], highlight the importance of pollutant accumulation in confined spaces and of evaluating air quality close to the pollutant source. When the breath is the pollutant source, the zone that characterizes it is designated BZ, for "Breathing Zone". The exposure of a subject, could be evaluated by measuring pollutant concentration in the BZ (either self-generated, as in our case, or from a different source).

The geometric extents of the BZ are a matter of debate. Haselton et al. [19] performed breathing visualizations through the nose using an artificial lung connected to a model of the human face. They concluded that the *zone of inhalation* can be represented as a hemisphere of radius 6.2 cm around the nose (~500 cm^3 in volume), while the exhalation can be represented by a 23° cone extending approximately 20 cm away from the nose (~350 cm^3 in volume). In studies concerning air quality in close proximity to humans, Brohus [20] reports that the BZ is habitually considered as a hemisphere of radius 30 cm (a volume of 56550 cm^3) centered on the human nose, drawing attention to the fact that the pollutant concentration is not constant in this sphere contrary to previous beliefs. This definition was adopted by the American Industrial Hygiene Association [21], the European Committee for Standardization (EN 15251 [22]), the U.S Dept. of Energy Guidelines [23] and recently EN ISO 18158 [24]. Melikov [25] recalls that this definition is inaccurate. Liden et al. [26] states that the 30 cm hemisphere is a technical definition based on the unlikely assumption of uniformity of concentration within this volume. Pantelic et al. [27] performed breathing measurements with human subjects in a zone of 30x60x50 cm (LxWxH), equivalent to a volume of 90000 cm^3. Air sampled in front of the nose led to the conclusion that there is significant variance in pollutant concentration between different points even for a single subject. Melikov [28], citing Haselton et al. [19] states that there is little difference between inhaling through the nose or through the mouth and subsequently states that while velocities can be high (without specifying a value) at the nose/mouth, they fall off rapidly after 2-3 cm. He further states that the majority of the inspired air comes from the convective boundary layer surrounding the body. The question remains open in the absence of gravity, where the convective boundary layer is absent.

Rim et al. [29] considered the BZ a volume of 500 cm^3 of unspecified geometry (likely parallelepipedal), with one of its corners centered on the nose tip. Rim et al. [29] state, as Melikov [28] previously did, that inhaled air mostly comes from the thermal boundary layer of the human body. Marr et al. [30] performed stereo PIV measurements in the breathing flow from the mouth, covering a rectangular region of 30x20 cm (HxL) in the median plane in front of the nose, tangential to the tip of the nose. Chen [31], states that the breathing zone is considered to be a cube with a 30 cm length (27000 cm^3) positioned with its corner centered on the nose. Recently Hweij et al. [32] and Assaad et al. [33–35] define the BZ as a sphere with a 2 cm diameter (a volume of 4.2 cm^3) situated 2.5 cm away from the nose, considering it the source of inhaled air.

Certain aspects are consistent throughout most of the studies: (1) the concentration is not uniform in the zone commonly designated by BZ when considering a large volume [20,22–24,27,31]; (2) the inhalation zone from which the air is drawn, considered as being more relevant for a definition of the BZ following the concept of uniformity of concentration, is of small dimensions with a volume in the 4.2 cm^3 [32] to 500 cm^3 [19,29] range, potentially varying between individuals. All the definitions of BZ or of "Inhalation zone", which are given in the literature deal with on Earth contamination problems.

Concerning our primary goal, the identification of the spatial distribution of exhaled CO_2 in the CQ, more precisely in the breathing zone, in connection with the breath's dynamics, we have the opportunity to define the breathing zone based on the dynamics of human respiratory cycles. The study was performed in a confined space in the absence of ventilation. The CO_2 accumulation was measured experimentally on Earth in a full-scale mockup of the CQ, and the resulting data were used to validate a numerical model. The validated numerical model was used to study the same phenomena in microgravity. The objective is (1) to understand the spatial distribution of CO_2 in the ISS CQ and (2) to investigate the geometric extents of the BZ with and without gravity. The BZ obtained with gravity will be compared to the numerous available definitions. The BZ without gravity will aid in reaching a clearer understanding of the possible deficiencies of the current ventilation system in the CQ, and to circumscribe the area that needs to be ventilated for the improvement of air quality in the astronaut's CQ.

2. Experimental Setup and Procedure

2.1. Experimental setup

A replica of the CQ was built for this study (Figure 1 a). The dimensions of the CQ and its ventilation system were extracted from its design documents [5,36,37], and the dimensions of the standard racks on the ISS [17]. The plywood walls were covered with layers of the same materials used as on the ISS for acoustic and radiation isolation purposes (NOMEX and Kevlar [18]).

Three NDIR CO_2 sensors (C1-C3), with a measurement range of 0-10000 ppm and a precision of ±50 ppm ±3% of reading with signal noise levels below 10 ppm, were installed inside the CQ model at different heights (Figure 1 b-e). The interior volume of the CQ is equal to 2.4 m^3. Each sensor was affected to one third of the total volume. Sensor (C1) is situated in the middle area of the model (Figure 1 b, c) at a height around the torso of the test subject, sensor (C2) was placed in the upper region of the model (Figure 1 b, d) and sensor (C3) was placed in the lower region (Figure 1 b, e). A fourth CO_2 sensor (C4) was installed outside adjacent to the CQ (Figure 2 a) to monitor exterior CO_2 levels.

Eight thermocouples were installed operating between -20 ÷ 60°C with an accuracy of ± 0.4°C between -20 ÷ 0°C and ± 0.1°C between 0÷60°C meant to verify the stability of the environment. Four thermocouples measured air temperatures (AT1-AT4) at the same positions as the CO_2 sensors (Figure 1 b-d). Another four measured interior wall temperatures (WT1-WT4) (Figure 2 b). One relative humidity sensor (RH1), with a range of 5÷98% RH with an accuracy of ±2% RH, was also placed at the same position as C1 (Figure 1 b and c), the closest position to the human head

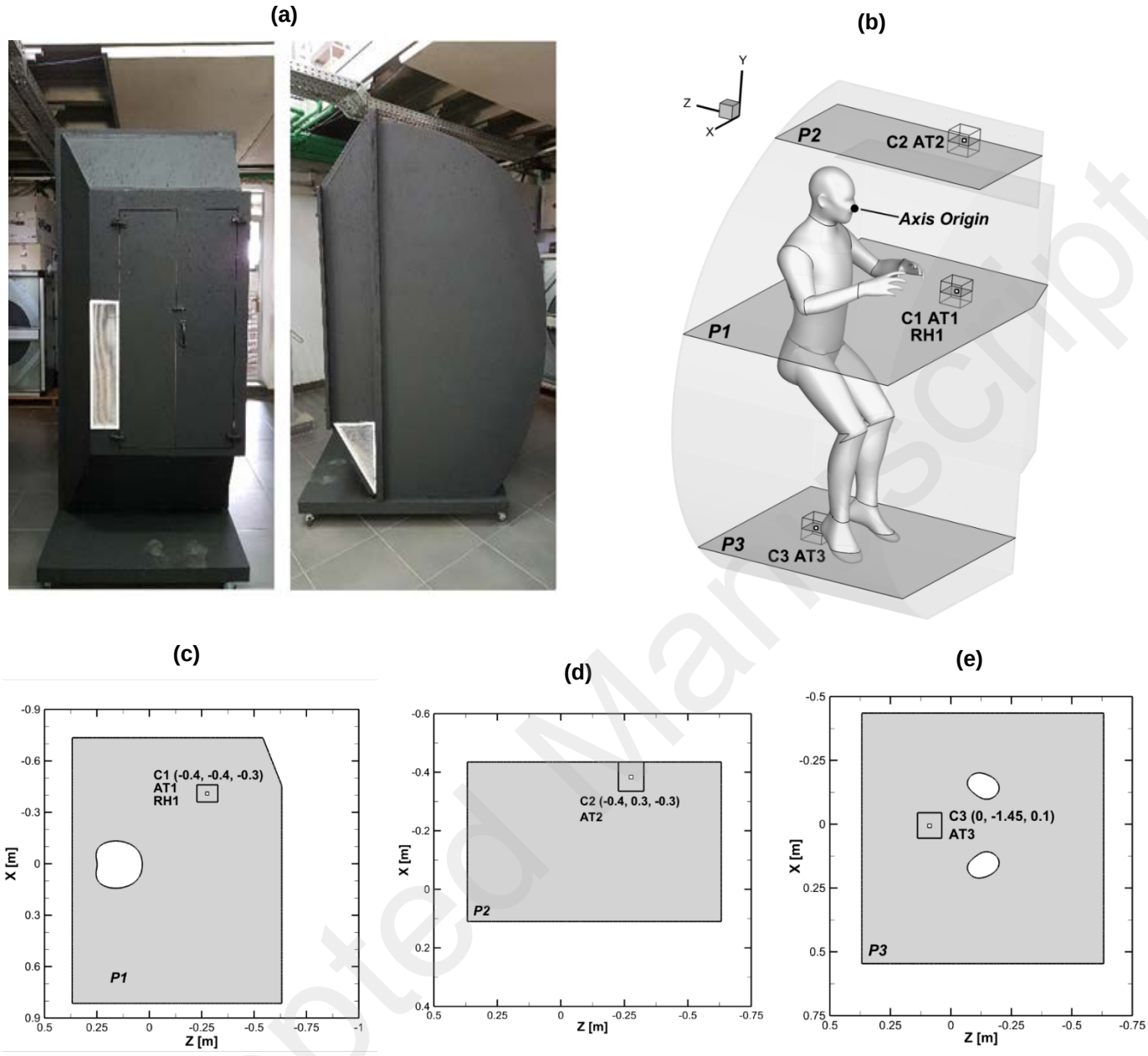

Figure 1 Laboratory mock-up representing the ISS CQ at 1:1 scale, Position of CO_2, Air Temperature and Relative Humidity sensors with planar coordinates: (b) 3D vision, (c, d, e) planes passing by sensors

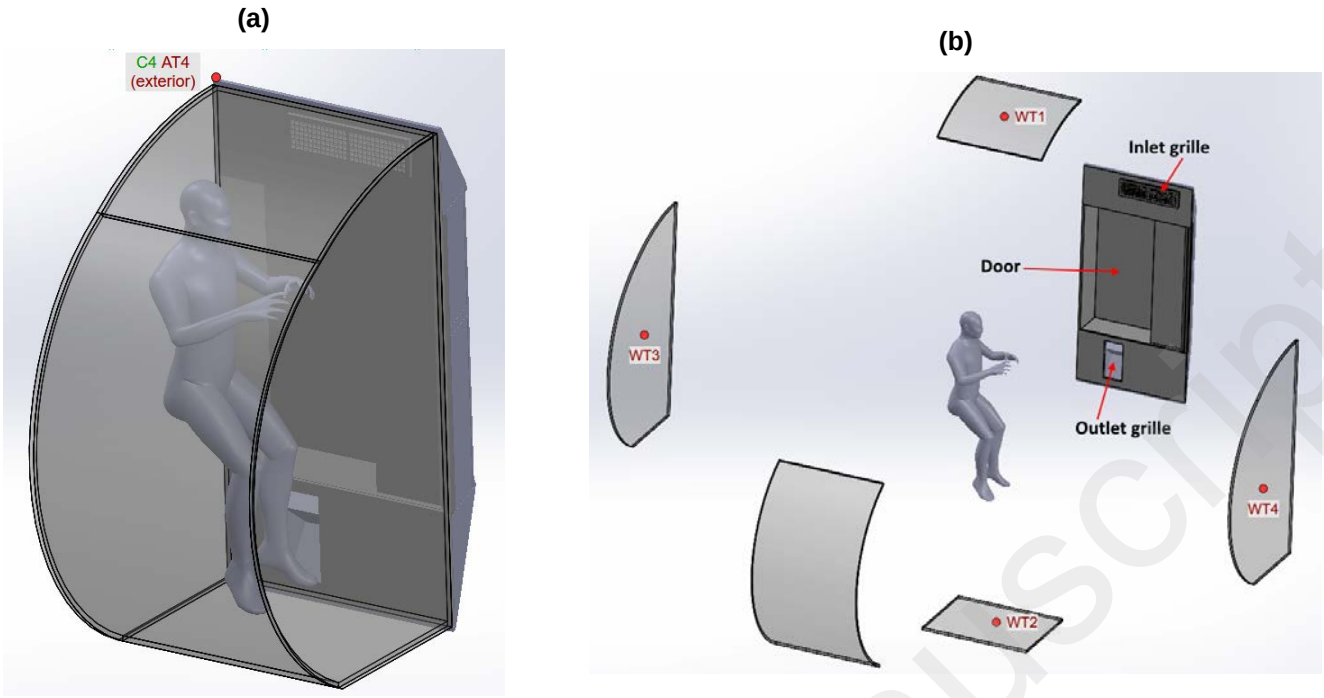

Figure 2 The test subject's position inside the CQ and the exterior CO_2 sensor's position (a); exploded view of the model with the positions of the WT sensors, the door and the inlet/outlet grilles of the general ventilation system (b).

The CQ replica was installed in a laboratory room where the air temperature, relative humidity and the CO_2 level were monitored. The average air temperature in the room was stable, at a value of 27°C with a standard deviation of ±1°C for all measurements. The relative humidity was 65% and the CO_2 level was found to be about 900 ppm. The indoor environment of the CQ model was at thermal equilibrium prior to testing. At the beginning of each test, conditions inside the CQ were the same as outside the CQ.

2.2. Experimental Procedure

A sample of 13 subjects was selected with ages in the 22-50 years interval, heights in the 1.65-1.89 m interval and weights in the 65-110 kg interval, 10 of them were males and 3 of them were females. This meets the recommendations of standard ISO 61010 [38], whereby a minimum of 8 subjects is needed for any sort of statistical evaluation of human-dependent phenomena.

Measurement time was limited to 15 minutes for health and safety concerns, with the subject inside the CQ model, the ventilation system deactivated and all openings sealed. Subjects were seated in a resting position, facing the wall featuring sensor WT4, on a modified chair, simulating the neutral posture of the body in microgravity. The subjects' feet did not touch the ground, similar to that of the human body, floating in microgravity. Subjects were instructed to count their number of breaths over a minute, 3 times during the test and to behave as they would normally while sitting at rest.

Prior to the tests, the subjects did not engage in significant physical activity and were kept for a period of about 10-20 minutes in the room where the CQ was placed, to ensure thermal acclimatization. Once the experimental procedure started, the CO_2 concentrations were recorded with a frequency of 0.5 Hz, while the temperature and relative humidity were logged with a frequency of 0.066 Hz. Over each of the 13 tests, exterior CO_2 levels measured by sensor C4 (adjacent to the CQ) remained constant, while interior CO_2 levels increased, indicating that no significant amount of CO_2 leaked from the CQ model. At the start of the tests, average wall and air temperatures were around 27°C, and the relative humidity was around 65%. At the end of the 15-minute testing period, both wall and air temperature sensors showed, on average, increases of about 1°C, and RH had risen to 70%.

Since the volume of the CQ is small (2.4 m^3) and the general ventilation system (Figure 2 b) is stopped during the experimental tests, the concentration measured in the sub-volume affected to each CO_2 sensor (C1, C2, C3) should reasonably approximate the average over that volume. The concentrations measured will be used to validate the average concentration levels in the numerical model, in the three respective sub-volumes. The method is

considered acceptable since the sensors measure CO_2 dispersion by natural convective mixing and diffusion while not directly influenced by the breath. The sensors were placed outside the area located in front of the test subject's head, to avoid the breath's influence.

3. Numerical Model and Boundary Conditions

The numerical model of the CQ (Figure 2) has a human model inside, resting in the neutral position of the body in microgravity, placed at the same height as the test subjects were seated during the experiments. Most of the subjects had heights around 1.80 m and the average value of all subjects' height was 1.79 m. The human model – if placed in straight position – has a height of 1.80 m. Its head features two nostrils, the inlets through which the realistic breathing process will occur.

The numerical grid has approximately 6 million tetrahedral elements with an average skewness of 0.22 and a wall $y^+ \approx 1$ for compatibility with a wide range of RANS turbulence models [39]. Five layers were created near the walls as shown in Figure 3. The darker regions represent a denser mesh around walls, areas with fine details such as the hands and around the nostril inlets (Figure 3 b, c).

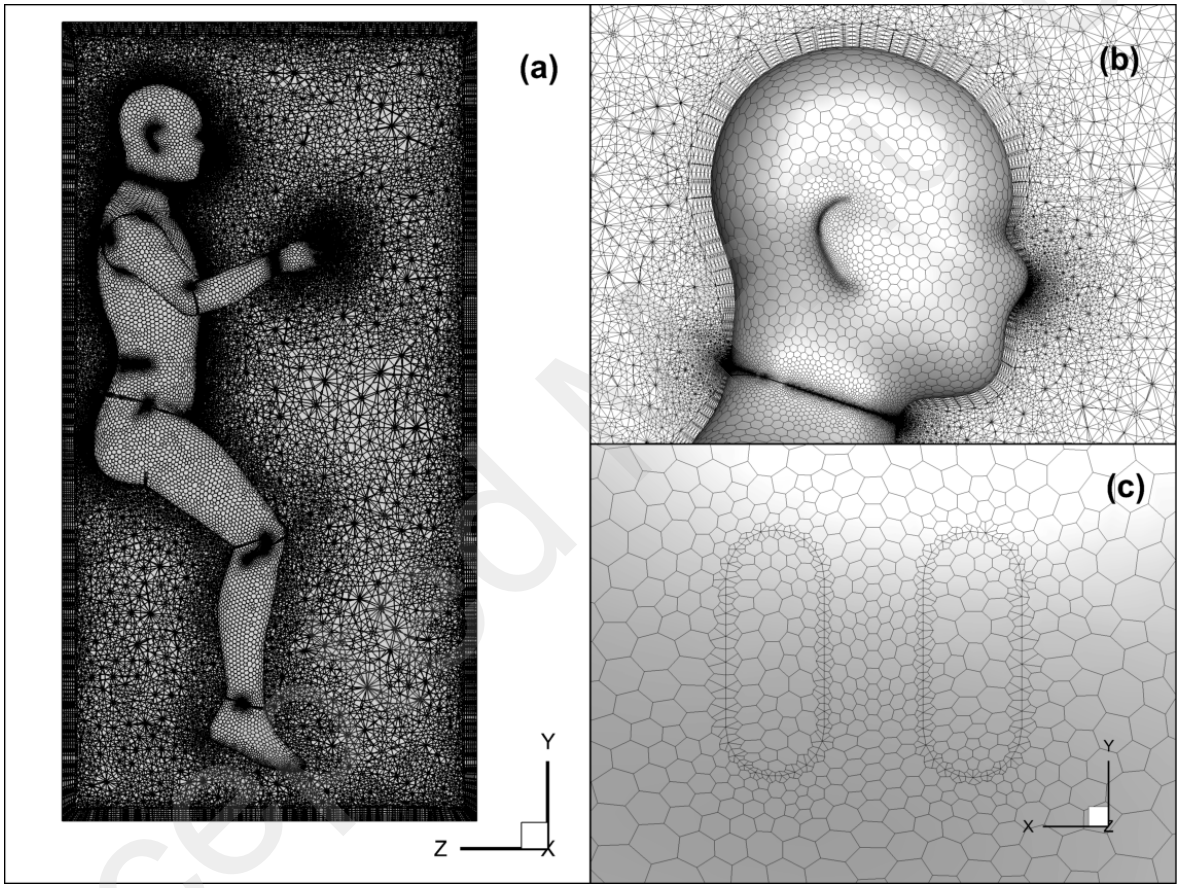

Figure 3 Mesh in the median plane of the human model (a), and details of the human head (b) and the nostrils (c).

The nostril's dimensions and their spacing were kept to realistic values, but because of the model design, their orientation is closer to parallel than previous literature reports [19,40].

The human breath is generally characterized by the volume of air that enters or exits the lungs with each breath termed Tidal Volume (V_t) [41], and the number of breaths over a minute (b_f). In emergency situations [42] V_t can be estimated by the individual's body weight and sex. The Pulmonary Ventilation Rate or Minute Volume (MV) [l/min] which represents the volume of air exhaled over one minute [43], is calculated as the product of V_t and b_f.

In our study, the breathing frequency is 14.7 breaths/minute (0.245 Hz), averaged over the 13 subjects, with an estimated [42] average tidal volume of 582 ml. MV (equivalent to exhalation/inhalation flow rates) can be computed as $MV = Q_{Exhaled} = Q_{Inhaled} = V_t * f\ [m^3/s]$ and used in determining the CO_2 generation rate, by subtracting the volumetric concentration of CO_2 in the inhaled flow (0.04%) from the concentration of the exhaled flow (4%) as follows:

$$CO_2\ generation\ = (Q_{Exhaled} \cdot 0.04 - Q_{Inhaled} \cdot 0.0004)\ [m^3_{CO_2}/s] \quad (1)$$

The result of Equation (1) multiplied by the test duration (15 min) falls within 5% of the overall CO_2 accumulation in the CQ after the experimental period giving confidence in the estimated value of V_t.

V_t, b_f, MV and Exhalation/Inhalation velocities were extracted from several studies of the human breath [44-45,50,56-57] and of the cross-infection risk in the built environment [46-49,51-55], for comparison with the present study in Table 1. The peak velocity at the breathing orifice is also given.

Table 1 Summary of the breathing parameters found in the literature.

	Type of study	V_t [ml]	b_f [min^{-1}]	MV [l/min]	Peak Exhalation/Inhalation Velocity [m/s]
Guyton and Hall [41]	Medical Manual	500	12	6	N/A
Adams [43]	Experimental	373	19.5	7.3	N/A
Bjorn, Nielsen [44]	Experimental and Numerical	600	10	6	N/A
Qian et al. [45]	Experimental	600	10	6	N/A
Olmedo et al. [46]	Experimental	570 / 660	19 / 15	10.8 / 9.9	4.74
Olmedo et al. [47]	Experimental	750 / 660	14.6 / 10	10.9 / 6.6	5.74
Cao et al. [48]	Experimental	550	16	8.8	3.4 ±0.3
Liu et al. [49]	Experimental and Numerical	~700	15	~10.5	No
Yoo, Ito [50]	Numerical	~555	14.8	~8.2	~ 2 – 4
Berlanga et al. [51]	Experimental	~570	~15.6	~8.9	~ 1 – 4
Cheng et al. [52]	Experimental	492	17.5	8.61	3.7
Average values	N/A	577	13 - 14	7.5 - 8	3.5 - 5
Present study	Experimental and Numerical	582	14.7	~8.5	5.49

In our study MV is approximately 8.5 l/min, and the peak exhalation/inhalation velocity is calculated at approximately 5.5 m/s (Table 1). V_t is almost equal to the average of the above studies, while the b_f, MV and velocity values fall in the ranges of the literature while slightly surpassing the average values.

In our CFD model, a breathing function was implemented, describing the breath through a sine function [53] as defined in Equation (2). This equation was determined based on $V_t = 582\ ml$, $f = 0.245\ Hz$ and the surface of the nostrils in our model $S = 0.8\ [cm^2]$.

$$u = u_{max} \cdot sin(2\pi ft) = 5.49 \cdot \sin(2\pi \cdot 0.245 \cdot t)\ [m/s] \quad (2)$$

In Equation (2) u [m/s] is the inlet velocity, u_{max} [m/s] is the maximum velocity when sin =1, f [Hz] is the breathing frequency and t [s] is the time. The sine function ensures both positive (exhaled) and negative (inhaled) airflow at the nostrils.

Our study requires a turbulence model (the nose's inlet Reynolds number is Re=3600 based on the peak exhalation velocity and the equivalent diameter of the two nostrils), a species transport model and an energy model for the heat transfer. After testing several turbulence models, the realizable k-ε model was chosen. In previous comparisons of turbulence models for the ventilation of the ISS Node 2 corridor, Smirnov et al. [16] found that the standard k-ε model offered acceptable results when compared to LES models, being adequate for studying the ISS environment. Enhanced wall functions were used for our study to ensure compatibility wall y^+ values close to 1 [39], addressing the limitations caused by the logarithmic functions describing the viscous sublayer in k-ε models. Although the sine-driven flow regime changes with the variable velocity, going from turbulent through transient and eventually to

laminar domains as it passes from the positive part of the sine function to the negative, previous studies of transient breathing functions [35] have obtained acceptable results using k-ε turbulence models.

A transient simulation was performed for a period of 60 s, with a time step of t=0.05 s, recording data at 0.1 s intervals. Each full breathing cycle lasts around 4 s (80 time-steps per cycle). The boundary conditions are presented in Table 2 and Table 3.

Table 2 shows the temperature and composition of the air inside the CQ and of the breath. Air was defined as a mixture of N_2, O_2, CO_2 and H_2O (vapors) volume fractions [$m^3_{component}/m^3_{mixture}$]. O_2 and CO_2 volume fractions in the ambient air are equal to the normal air composition on Earth – 21% O_2 and 0.04% CO_2 (equivalent to 400 ppm CO_2). H_2O volume fraction was chosen so that the RH at the start of the simulation would be equal to 65% as measured in the experimental study. The N_2 volume fraction is automatically computed so the sum of all volume fractions equals unity. Ambient air temperature was set at 27°C (the initial value of the experimental study). The CO_2 concentration of 400 ppm is not equal to that of the experimental measurements, because of the assumptions made in Equation (1). This will not be a problem, since the objective is the study of accumulation and both experimental and numerical CO_2 curves will have their initial value subtracted so that they start from 0.

During exhalation O_2 and CO_2 volume fractions were set to their habitual values in the exhaled air [41], 15% O_2 and 4% CO_2 (Table 2). The H_2O volume fraction was chosen so that RH would reach 100% as stated in the medical literature [41] and supported by other studies concerning the simulation of the breath [44], [54], [49]. Air temperature was set to 36°C, the same temperature as the human head. Nostril velocity is governed by Equation (2). During the simulation, ambient parameters change, and air is inhaled at ambient temperature and gas concentrations. This differs from the assumptions of Equation (1), but its effect on exhaled CO_2 concentration is not felt over short periods of time [41].

The wall temperature of the CQ is 27°C (Table 3) as at the start of the experimental study, the temperatures on the different human body parts have been selected from ASHRAE's recommendations [55] for the skin temperatures of an average human. It was not possible to measure the skin temperature of the test subjects for fear of inducing stress and potentially altering the CO_2 generation rate.

Table 2 CQ ambient air parameters and nostril inlet boundary conditions

	Boundary condition	T [°C]	O_2 volume fraction [-]	CO_2 volume fraction [-]	H_2O volume fraction [-]	Velocity [m/s]
Ambient air	-	27	0.21 (21%)	0.0004 (0.04%)	0.0244 (2.44%)	-
Nostrils during exhalation	Velocity inlet	36	0.15 (15%)	0.04 (4%)	0.0615 (6.15%)	$u = 5.49 \cdot \sin(2\pi \cdot 0.245 \cdot t)$
Nostrils during inhalation	Velocity inlet	Ambient values				$u = 5.49 \cdot \sin(2\pi \cdot 0.245 \cdot t)$

Table 3 Wall and human body surface boundary conditions [55]

Region	Walls	Head	Torso	Arms	Forearms	Hands	Lower abdomen and thighs	Shins	Feet
T [°C]	27	36	34.5	33	32	30	32.5	30	27

The Coupled pressure-velocity algorithm was used, with a second-degree discretization scheme. Convergence criteria were set to reach the order of e-6 for all equations. Satisfactory convergence was reached upon the plateauing of the residuals after 50 iterations. Convergence was monitored by the mass flow rate on the inlet nostrils, the CO_2 volume fraction variation on the nostrils and in the CQ overall.

Two numerical simulations were performed, one reproducing the experimental conditions ($g = 9.81\ m/s^2$) and another identical one with $g = 0\ m/s^2$ to reproduce microgravity conditions. The simulation without gravity was not meant to evaluate the CO_2 concentration at the end of an astronauts' sleeping period in the CQ, but to highlight the regions of CO_2 accumulation due to their breath.

4. Results and Discussion

4.1. Analysis of the numerical carbon dioxide accumulation in the CQ with and without gravity

CO_2 accumulation inside the CQ during experimental observation for all test subjects is given in Figure 4 a_1-c_1. A zoom is given for the first minute of observation in Figure 4 a_2-c_2.The initial CO_2 concentration [mg/m^3] was extracted from each measured concentration so that all curves start from 0. This result was multiplied by the volume affected to each sensor in order to obtain the quantity of CO_2 [mg] at the initial time t_0, named $CO_2(t_0)$ [mg].

The difference between the quantity of CO_2 [mg] at time t and the same quantity at the initial time (t_0) was termed $CO_2\ \ accumulation$ (Equation 3).

$$CO_2\ accumulation\ (t) = \ CO_2(t) - CO_2(t_0)\ [mg] \qquad (3)$$

The continuous black line on the graph (Figure 4 $a_{1,2}$-$c_{1,2}$), corresponds to the best fit of $CO_2\ accumulation$ over all the points measured by each sensor for the 13 subjects, during the 15-minute duration of the test. The good regression coefficients attest to the linearity of the CO_2 accumulation phenomenon, as expected in the case of breathing inside a room without ventilation [56].

The human in our numerical model is static unlike the test subjects making punctual comparisons difficult. Consequently, for the numerical validation it was decided to affect the three sensors to three roughly equal fractions of the total CQ volume: one corresponding to the top region for C1, one to the middle for C2, and one to the bottom for C3. Hence, C1, C2 and C3 will represent either sensors or their corresponding volumes.

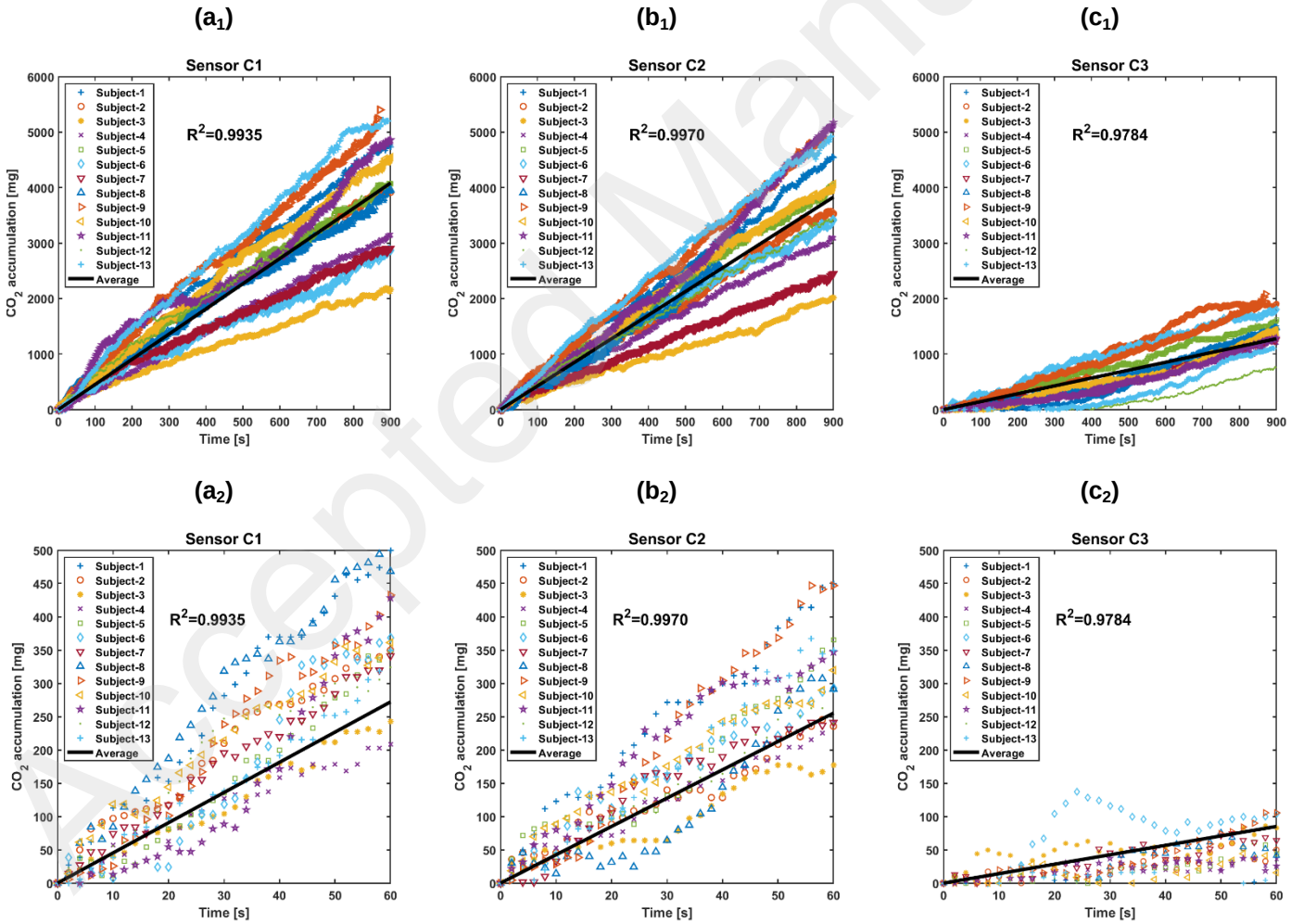

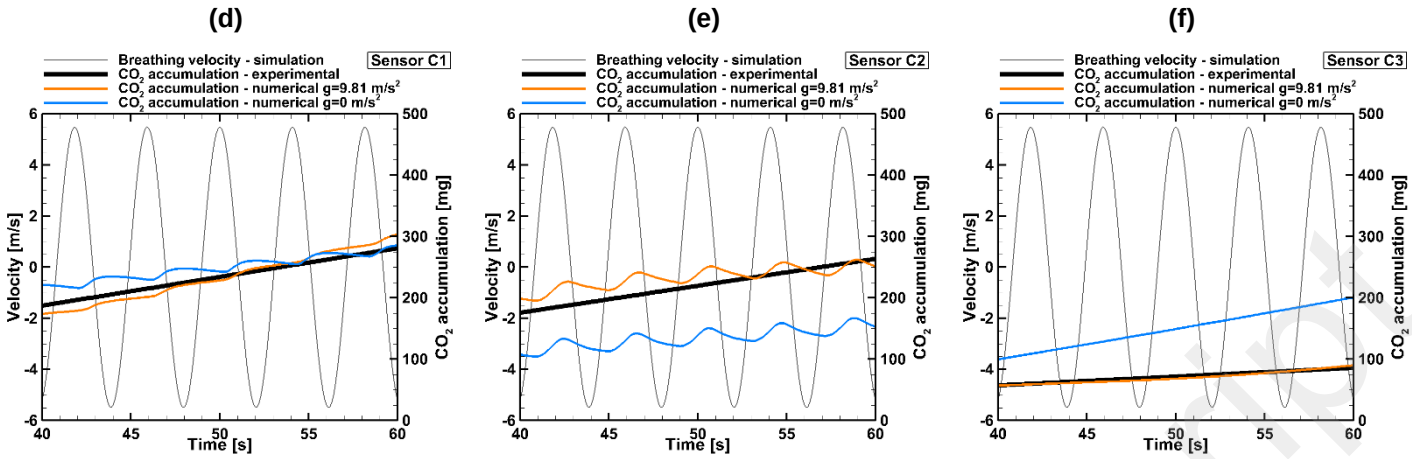

Figure 4 CO_2 accumulation in the experimental model over 15 minutes for sensors C1 (a_1), C2 (b_1) and C3 (c_1) as well as over 60 s (a_2, b_2, c_2); numerical and experimental CO_2 accumulation data at sensors C1 (d), *C2* (e), *C3* (f) – breathing velocity function superposed for investigating imprints on CO_2 accumulation.

The experimental best fit curves (Figure 4 a_2-c_2) are reported on Figure 4 d-f where the comparison with the numerical model covers the last 20 seconds (~5 full breathing cycles) of the simulated duration of 60 seconds. This choice was made to allow the exhaled CO_2 to disperse inside the numerical model for the first 40 seconds of the simulation. In Figure 4 d-f, the numerical CO_2 accumulation curves with and without gravity are plotted on the same graphs as the nostril breathing velocity, to highlight possible correlations between them.

For the three volumes, numerical CO_2 accumulation with gravity is in agreement with the experimental data (Figure 4 d-f). The CO_2 has a sharper slope at sensor C1 because the sensor's affected volume is below head level in the direction of the exhaled CO_2. The undulations visible on the numerical curves relative to volumes C1 and C2 are imprints of the breathing cycle upon the CO_2 accumulation curves. The low time resolution of the CO_2 sensors used in the experiments does not capture such undulations. The curve relative to volume C3, the furthest from the breathing zone, does not show any undulation. The influence of the breathing cycle in Figure 4 d has a slight phase delay from what is seen in Figure 4 e, because the nose is situated in the volume fraction attributed to sensor C2 where the influence of the breath is sensed immediately.

Numerical results without gravity have a similar ascending tendency (Figure 4 d-f). Without gravity, C1 presents no significant difference relative to the case with gravity (Figure 4 d). Without gravity, C2 (Figure 4 e) presents a 40% deficit of CO_2 at t=60 s compared to the case with gravity (caused by the absence of natural convective flows). The exhaled CO_2 is driven solely by the momentum of the breath, directing it towards the bottom of the CQ. At C3 (Figure 4 f), the case without gravity presents a surplus of CO_2 accumulation. The ≈100 mg surplus found at t=60 s in C3 is quantitatively identical to the deficit present around C2.

The numerical CO_2 accumulation in the total volume of the CQ is almost identical with and without gravity (0.1% difference). The difference between numerical and experimental CO_2 accumulation is around 6% in favor of the experiment, considered acceptable.

Table 4 Experimental-numerical comparison of air temperatures (AT sensors) and their variation over 60 s

	Time	Temperature [°C]		
		AT1	AT2	AT3
Experimental	t = 0 s	27.4	27.6	27.5
	t = 60 s	27.5	27.9	27.5
Numerical	t = 0 s	27.7	27.7	27.7

(g=9.81 m/s^2)	t = 60 s	27.8	28.4	27.7

Table 4 presents average temperatures over the C1-C3 volumes for the numerical simulation compared to experimental sensors AT1-AT3 at t_0 and t=60 s. Over this interval, temperatures for AT1 rose with 0.1°C in both the experimental and the numerical cases, while for AT2 they increased by 0.3°C in the experimental case and 0.7°C in the numerical simulation. AT3 shows no change in both experimental and numerical cases. Average wall temperatures experimentally recorded by sensors WT1-WT4 were 27°C showing changes ≤0.1°C over 60 s. This is within their accuracy range (±0.1°C between 0°C and 60°C) and were thus considered constant in the timeframe of the CFD simulation.

RH values in the experimental measurements increased on average by 0.7% for the 13 subjects over 60 seconds. This value is lower than the accuracy of the sensor (±2%), thus for the 60-second time interval used in this study it is considered to remain constant. The numerical model shows a low increase of 0.1% in RH after 60 seconds.

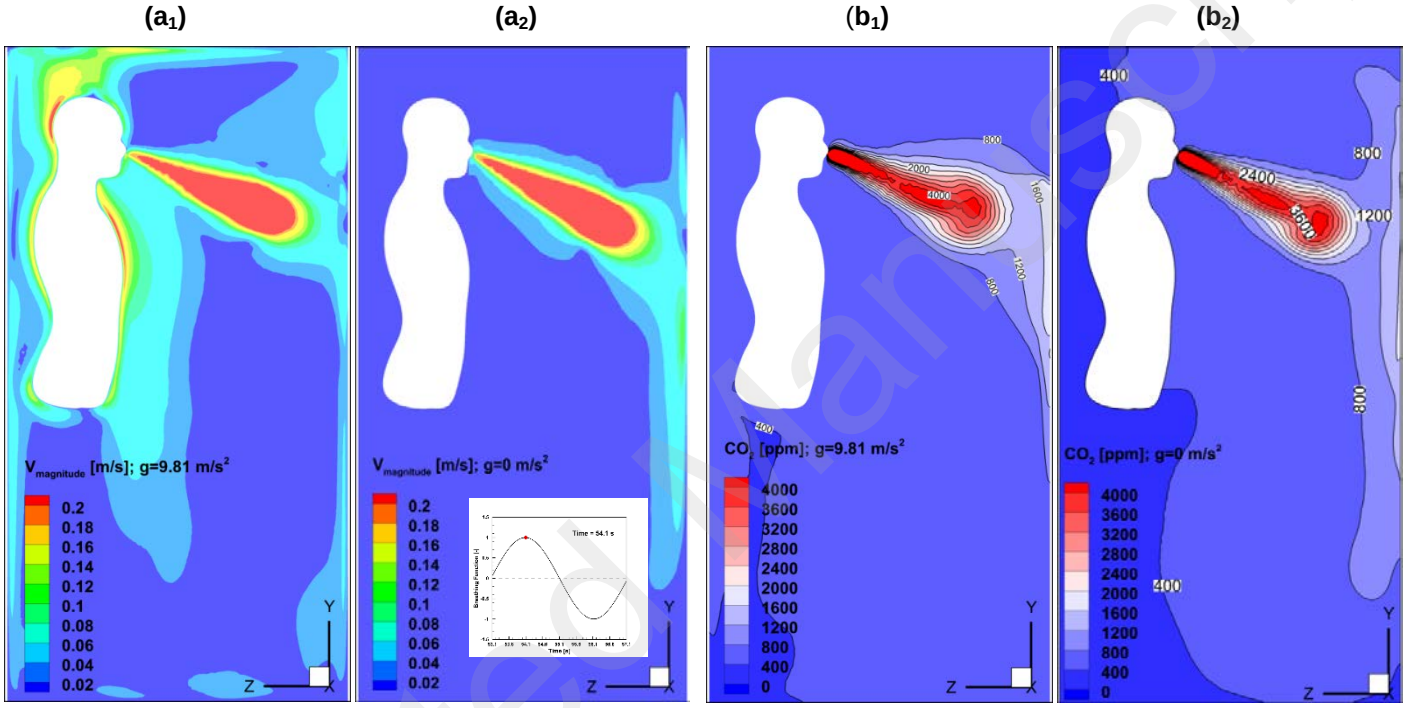

Figure 5 Velocity magnitude contours (a_1, a_2) and spatial distribution contours of CO_2 $concentration$ $[ppm]$ (b_1, b_2) for the cases with and without gravity.

Given the agreement between the numerical and the experimental results with gravity, the numerical model was considered to be validated, giving confidence in the numerical results obtained without gravity aimed at studying microgravitational effects on the spatial distribution of CO_2 in the CQ.

Velocity fields at the exhalation's peak in the breathing cycle are given in Figure 5 a1, a2 for cases with and without gravity. When gravitational acceleration is present (Figure 5 a1), the thermal plume of the human body can be observed. In the convective boundary layer around a simulated human at 5 cm in front of the neck, chest, and upper legs, Cheng et al. [52] found values in the range of 0.05 m/s-0.12 m/s, which compare well with our results. In Figure 5 a1 the plume is seen interacting with the breathing jet in its low velocity top region, producing a recirculation in the top of the CQ. Without gravitational acceleration (Figure 5 a2), the breathing jet behaves similarly to an inclined impacting jet, reaching the opposite wall unimpeded and dispersing upon impact. The spatial distribution of CO_2 is closely related to the velocity fields (Figure 5 b1, b2). CO_2 preferentially accumulates in the upper regions of the CQ in the case with gravity (Figure 5 b1), while without gravity (Figure 5 b_2) the CO_2 contours follow the velocity distribution of the impinging jet very closely. These observations are in agreement with the global results given in Figure 4 d- f. Without gravity, there is less mixing of CO_2 in the CQ and regions with CO_2 $concentration < 400\ ppm$, almost inexistent in the case with gravity, occupy almost a third of the CQ volume when $g = 0\ m/s^2$ (Figure 5 b_1, b_2).

A direct comparison of the cases with and without gravity is given by the difference ΔCO_2 (Figure 6) between the CO_2 $concentration$ [ppm] distributions with and without gravity respectively. The resulting fields are plotted at four key instants of the breathing cycle. Positive values of ΔCO_2 indicate higher concentrations without gravity than with gravity, and the corresponding regions are correlated to the trajectory of the breathing jet. The negative zones could be roughly associated with zones of low velocity where buoyancy plays a role in the airflow, as per the case with gravity. Absolute ΔCO_2 levels in the breathing flow are variable during the breathing cycle, high values are recorded during the exhalation phase (Figure 6, a, b) and low values during the inhalation phase (Figure 6, c, d). Regions far away from the nose do not show significant changes of ΔCO_2 during the breathing cycle.

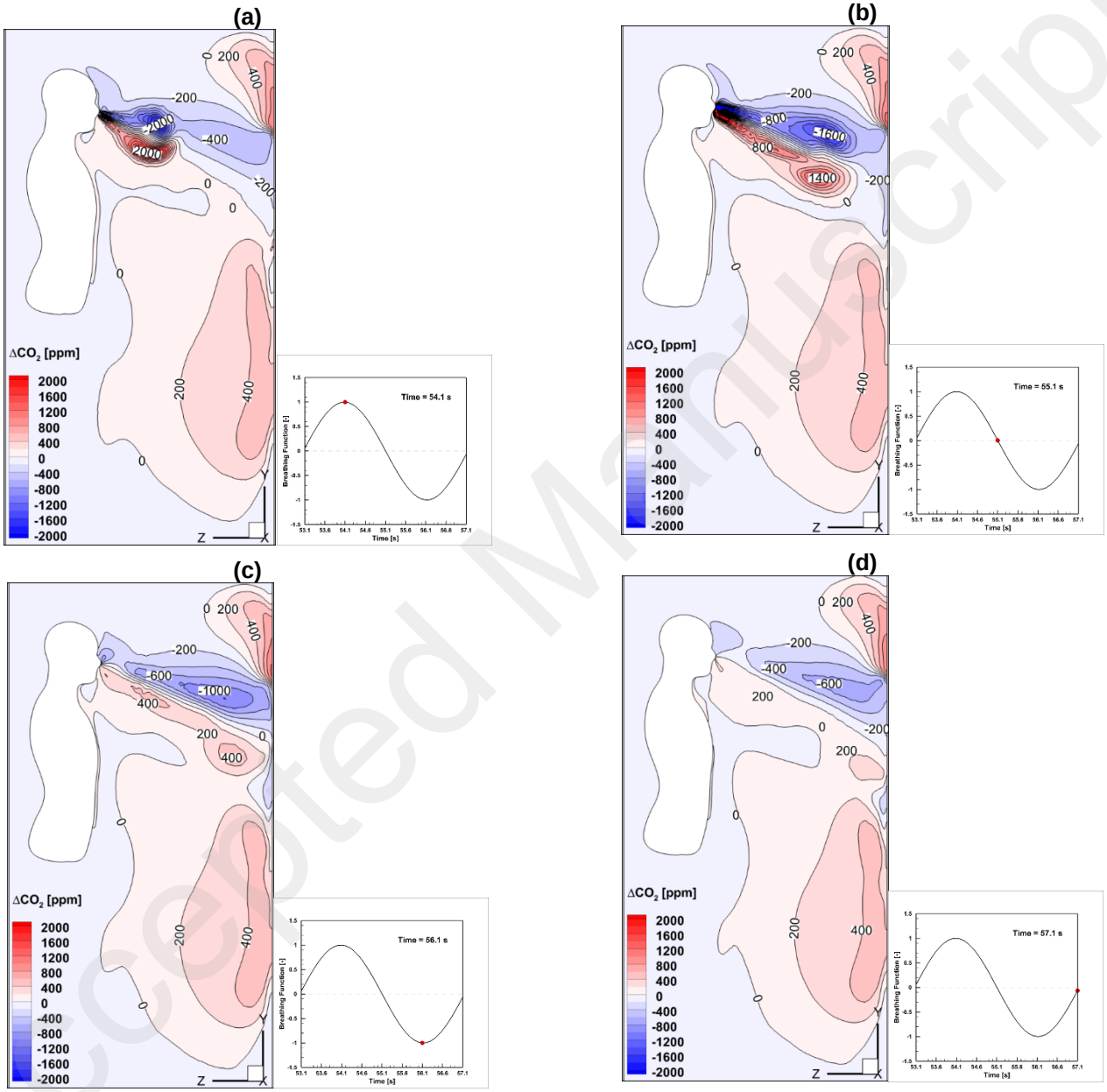

Figure 6 Difference between the CO_2 $concentrations$ of the no-gravity case and the CO_2 $concentrations$ of the case with gravity, at different instants of breathing cycle.

The authors' investigation of the general ventilation system of the CQ (not detailed for brevity) indicates that CO_2 accumulates in poorly ventilated regions where air stagnates. This will be detailed in future research. Currently the focus is on a precise definition of the BZ to be targeted by future ventilation solutions.

4.2. Dynamic analysis of the breathing flow

The numerical breathing flow, obtained with gravity, is compared to the experimental data of Yao et al. [57], where a manikin breathed through a circular orifice (the mouth), 12 mm in diameter, generating a single round jet. To our knowledge, there is no similar experimental data in the literature for breathing through the nostrils. In our case, each elliptic nostril has an equivalent diameter d_e=7 mm. The equivalent diameter of the two nostrils is D_e=11 mm (close to study [57]). While d_e would be relevant for analyzing the interaction of the near field of nostril jets, D_e is relevant for the analysis of the far field, where the flow behaves as a round jet coming from a single round orifice of diameter D_e. It is possible to compare our numerical breathing flow to that of [57] in the far field, by normalizing distances by D_e, as the authors have, and by the normalized streamwise velocity W^B/W^B_0 in the breathing plane BP (Figure 8 a), where W^B_0 is the streamwise velocity at the nostril opening. Fields were extracted at the same instants observed in [57] (Figure 7 b-f).

For comparison, we retain instant t_2= 54.1 s (Figure 7 d) corresponding to the developed exhalation, for which the far field exists. In the near field, the twin nostril jets are clearly visible. The velocity profile presents two maximums (W^B_{max}) on either side of a central minimum (W^B_C). This double hump profile disappears after a few diameters D_e, and from this distance, the flow resembles a round jet coming from an orifice of diameter D_e. Yao et al. [57] present the field for a maximum distance of 8 D_e, where the normalized velocity of 0.25 compares well with our result at 8 D_e. The dynamic expansion, based on a normalized velocity W^B/W^B_0 = 0.1, at a value of $\pm$ 1 D_e and a normalized distance of 8 D_e, is similar to the literature results [57].

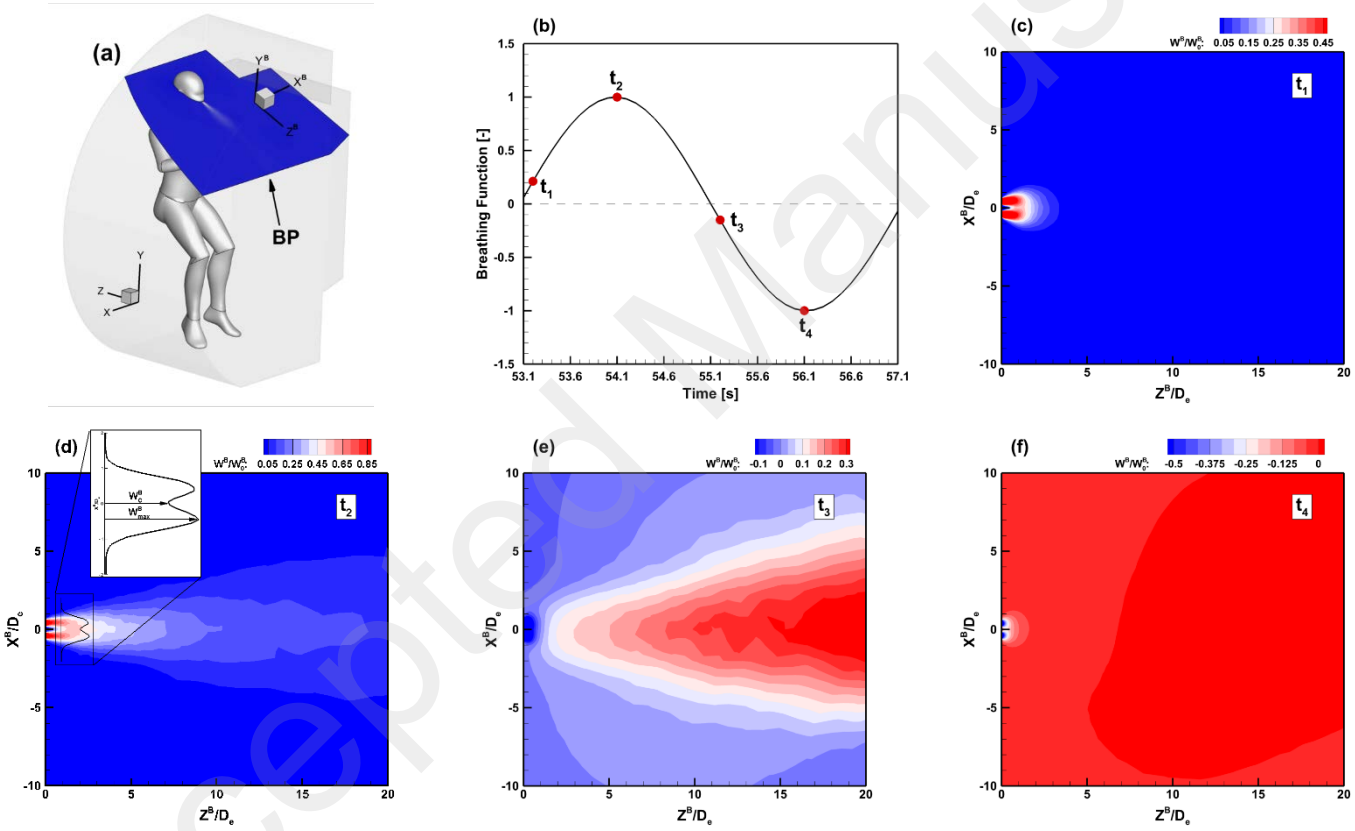

Figure 7 The breathing plane – BP (a), a breathing cycle (b), nostril twin-jet velocity fields at different instants of the breathing cycle (c-f) in plane BP with gravitational acceleration

Streamwise centerline velocity W^B_c and streamwise maximum velocity W^B_{max} are plotted in Figure 8 a,b, at peak exhalation (t_2=54.1 s), and peak inhalation (t_4=56.1 s).

The velocity fall-off (3 cm from the nostrils) considered by Melikov [28] is represented by a vertical dashed line in Figure 8 a, b. It is situated immediately after the position where W^B_c begins to decrease on the peak exhalation velocity curve. The peak inhalation velocity drops to near 0 after the 3 cm limit.

The BZ as defined by Hweij et al. [32] (a 1 cm radius sphere, 2.5 cm in front of the nose) is represented in Figure 8 a, b by a pink line. The exhalation zone (a 23° angle cone extending up to 20 cm, represented with a red line) and the inhalation zone (a 6.2 cm radius hemisphere represented with a blue line) of Haselton et al. [19] were

superposed as well. The intersection between the exhalation cone and the inhalation hemisphere of Haselton et al. [19] (the hatched zone in Figure 8 a, b), corresponding to the zone where the exhaled air is rebreathed, compares well with the BZ of Hweij et al. [32]. The 30 cm hemisphere representing the BZ according to Brohus (represented with a black dotted line) [20] covers all of the previous. At its border $W^B_c = W^B_{max} \approx 0$ m/s.

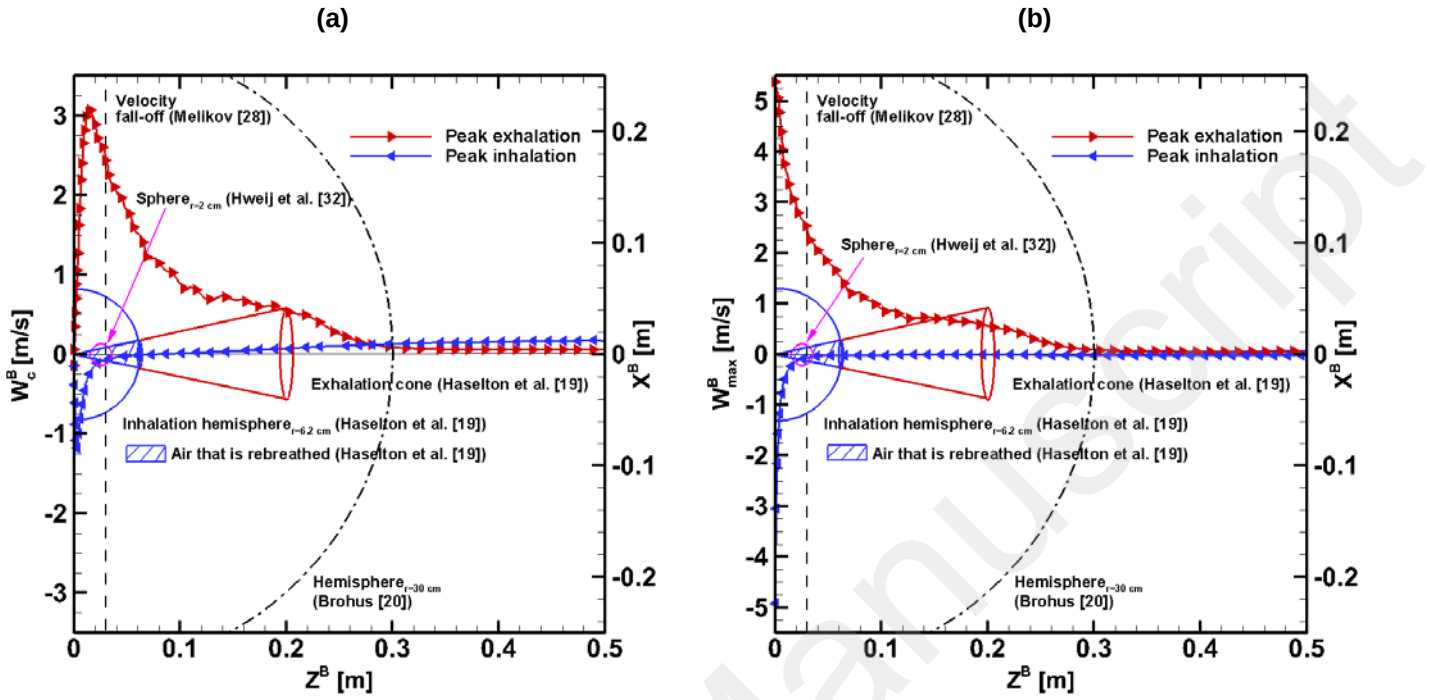

Figure 8 Streamwise central (a) and maximum (b) velocities in the breathing flow, superposed to the breathing zone definitions.

With the many different definitions of the BZ identified above we wanted to check if the entire sine dynamics of breathing (as opposed to instants in time) could be used to obtain a rigorous definition of the BZ, with and without gravity.

Our approach studies the Fast Fourier Transforms (FFTs) of the main velocity component of the breathing flow W^B in the amplitude-frequency domain. Taking the FFTs of the corresponding velocity in a spatial point over time, if a peak is found at the breathing frequency ($f_0 = 0.245\ Hz$) or at a multiple of this frequency, that point is considered sensitive to the breathing jet.

Two fixed planes were considered for this analysis: plane BP already defined in Figure 7 a and the vertical median plane MP passing through the middle of the head (Figure 9 b). Lines L^{BP}_i and L^{MP}_i were generated using a mobile frontal plane FP_i perpendicular to BP. When FP_i intersects BP (Figure 9 a), a line L^{BP}_i is generated and when FP_i intersects MP a line L^{MP}_i is generated (Figure 9 b). 31 L^{BP}_i and 31 L^{MP}_i lines were generated as shown in Figure 9 c. For i=1…4, the distances to the nostrils are given. For i>4, the distance increases in increments of 2.5 cm up to a distance of 70 cm.

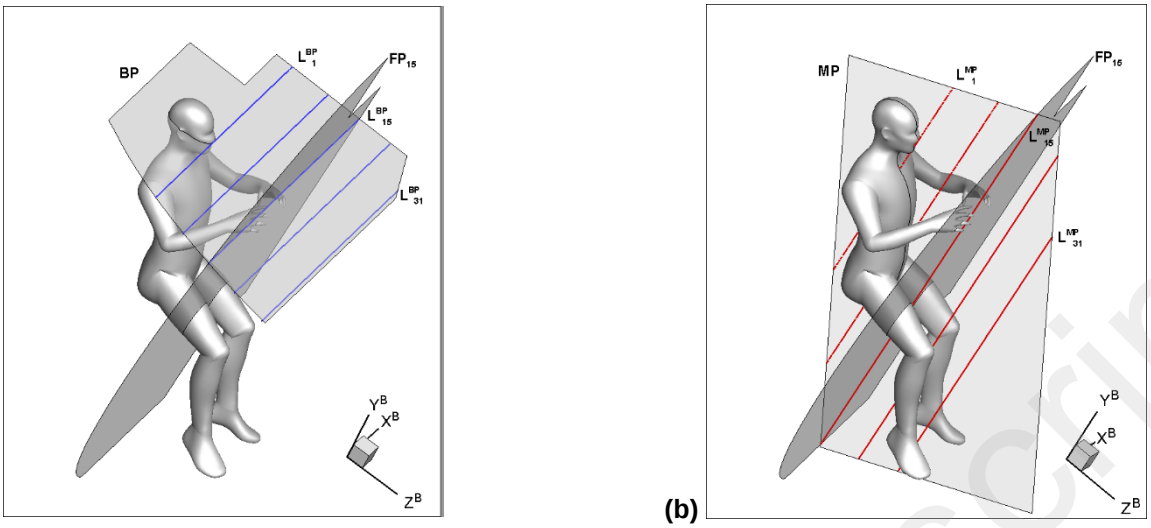

(c)

L^{BP}_i generation	L^{MP}_i generation	Distance Z^B from nostrils
$L^{BP}_1 = BP - FP_1$	$L^{MP}_1 = MP - FP_1$	0 cm
$L^{BP}_2 = BP - FP_2$	$L^{MP}_2 = MP - FP_2$	0.5 cm
$L^{BP}_3 = BP - FP_3$	$L^{MP}_3 = MP - FP_3$	1.25 cm
$L^{BP}_4 = BP - FP_4$	$L^{MP}_4 = MP - FP_4$	2.5 cm
...	...	...
$L^{BP}_{31} = BP - FP_{31}$	$L^{MP}_{31} = MP - FP_{31}$	70 cm

Figure 9 Lines L^{BP}_i (a) and L^{MP}_i (b) for BZ investigation. (c) the generated lines and their positions relative to the nostrils.

FFTs of W^B along the L^{BP}_i lines will delimit the zone influenced by the breath along the X^B axis, while FFTs of W^B along the L^{MP}_i lines will delimit the zone along the Y^B axis. The zone's depth along the Z^B axis will be determined by the maximum amplitude of the FFTs at f_0 from $L^{BP}_{1\text{-}31}$ or $L^{MP}_{1\text{-}31}$. Theoretical limits of FFT amplitude (both superior and inferior) must be determined, to evaluate how closely the signal follows the breathing function.

Three limits were determined in Figure 10 d-f, $l_{(1)}$ the theoretical upper limit (Figure 10 d), indicating perfect synchronization with the sinewave in Equation (2) (Figure 10 a), $l_{(2)}$ an intermediate limit (Figure 10 e) obtained by taking the FFT of the positive half of the-sine wave (Figure 10 b, considering the negative half leads to an identical result); $l_{(2)}$corresponds to a weaker influence of the breathing cycle or to solely the exhalation or inhalation part of the cycle. $l_{(3)}$ is the lower limit (Figure 10 f) below which the breathing cycle is not felt, computed as the average maximum amplitude of several white noise signals (Figure 10 c).

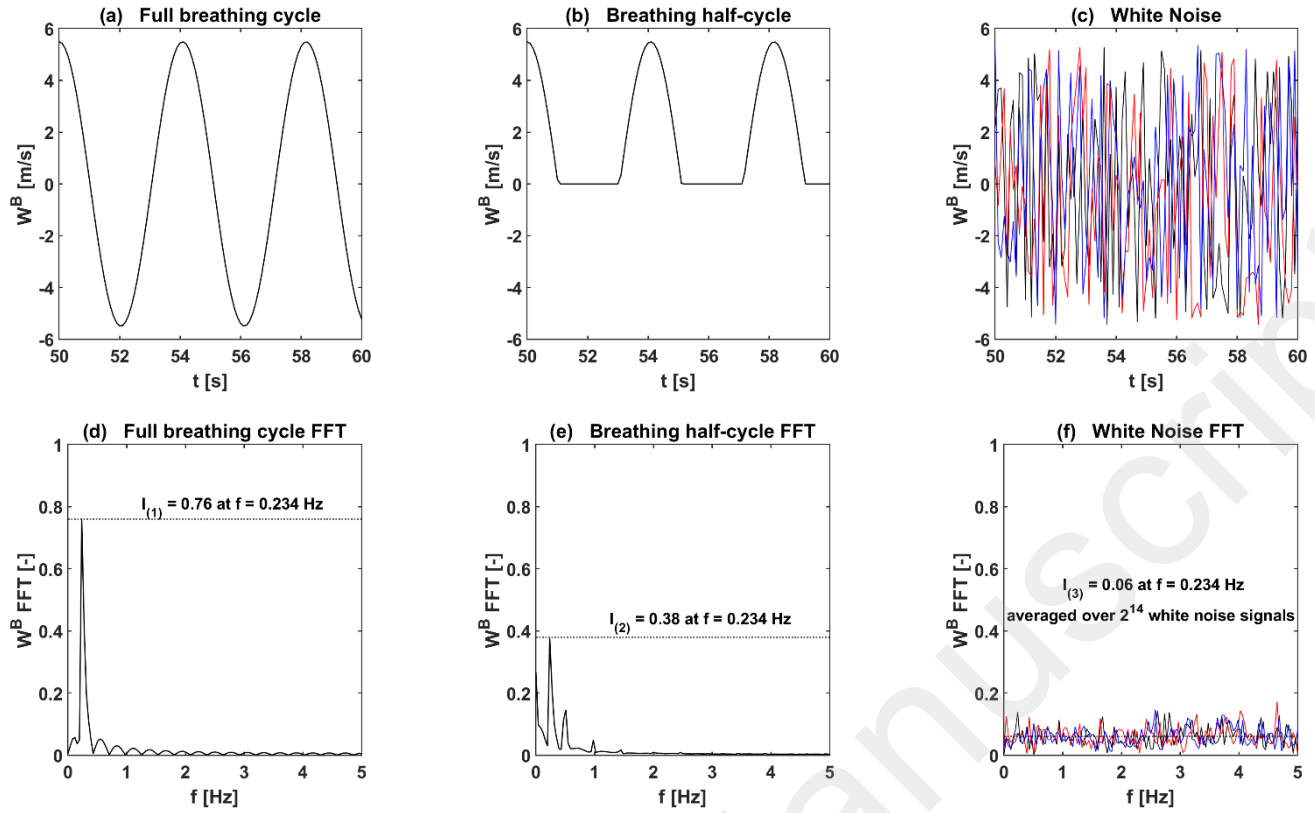

Figure 10 Normalized FFT limits for the full breathing cycle (a, d), the breathing half-cycle (b, e) and random white noise signals (c, f).

The FFT of Equation (2), at a frequency of 10 Hz (the 0.1 s time step of the simulation), results in a peak at $f = 0.234\ Hz \cong f_0$. For comparison, the results FFT(W^B) are normalized by the maximum amplitude of the velocity function given by Equation (2), which is W^B_0 (t_2) = 5.49 m/s. In the following FFT(W^B)/W^B_0(t_2) will be designated by FFT_N, leading to an upper limit $l_{(1)} = 0.76$, an intermediate limit $l_{(2)} = 0.38$ and a lower limit $l_{(3)} = 0.06$ of FFT_N (Figure 10 d-f).

The FFT analysis was performed from L^{BP}_1 to L^{BP}_{31} and L^{MP}_1 to L^{MP}_{31} for both numerical cases. Beyond L^{BP}_7 and L^{MP}_7 the maximum amplitudes at f_0 fell below the white noise limit $l_{(3)}$. FFT_N amplitudes were extracted at f_0 and plotted in Figure 11 along with limits $l_{(1)}$, $l_{(2)}$ and $l_{(3)}$. Line L^{MP}_1 does not appear in this figure because it is tangent to the wall between the nostrils (Figure 9 b). For interpretation, the authors have made the following assumptions: FFT_N amplitudes between $l_{(1)}$ and $l_{(2)}$ correspond to a strong influence of the full breathing cycle (exhalation and inhalation) while amplitudes between $l_{(2)}$ and $l_{(3)}$ are representative of a half-cycle (solely exhalation or solely inhalation) or a weak influence of the full cycle. Amplitudes below $l_{(3)}$ correspond to white noise and were ignored.

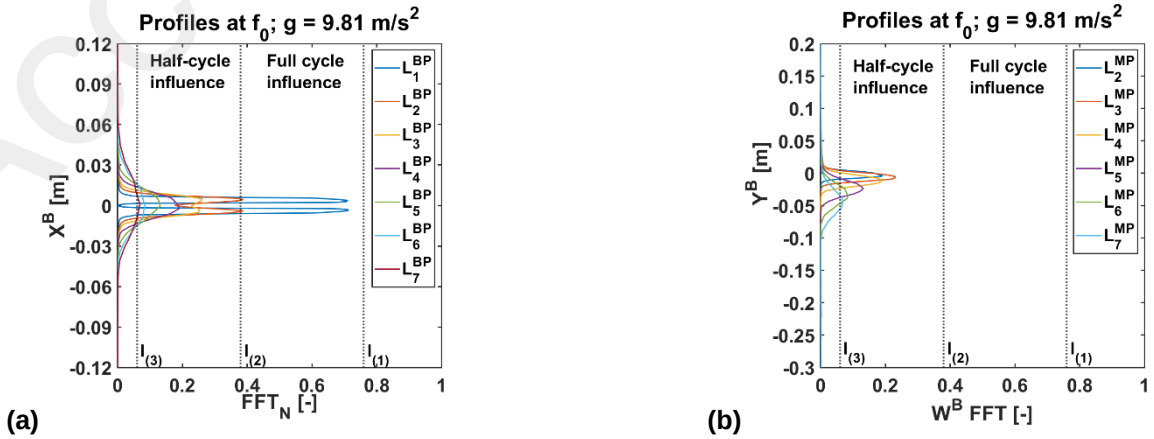

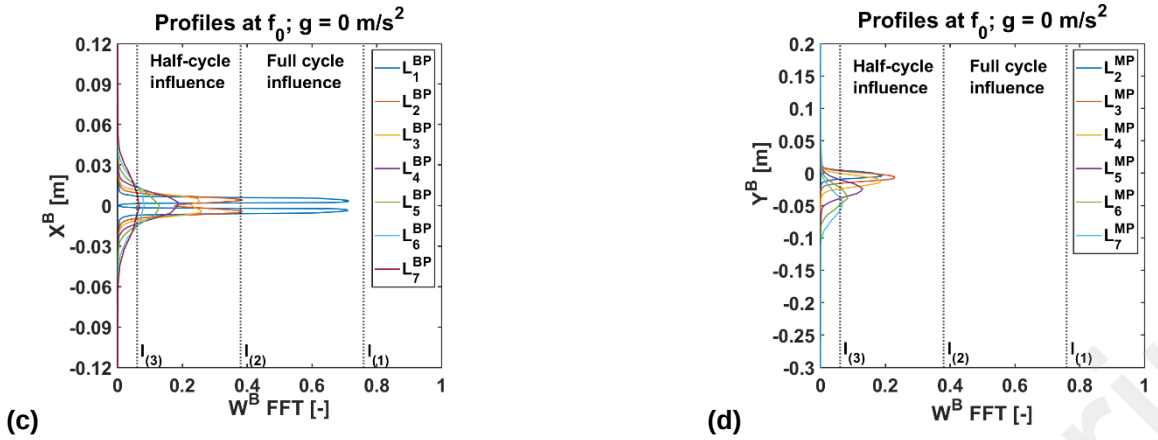

(c) **(d)**

Figure 11 FFT_N amplitudes at $f_0 = 0.234\ Hz$, with (a, b) and without (c, d) gravitational acceleration.

After delimiting the curves (see Figure 11) along the X^B and Y^B axes, the resulting zones influenced by the breathing cycle are presented in Figure 12 a,b and are superposed to W^B_{av} (W^B averaged over one breathing cycle) fields. The yellow line in Figure 12 a represents the zone influenced by the full breathing cycle (zoom highlighted in Figure 12 a), it extends 0.5 cm in front of the nostrils and corresponds to the highest velocities at peak exhalation and inhalation.

The dotted black zone, contiguous to the yellow one, influenced by the half breathing cycle, considered as the BZ, takes a diamond-like shape, extending up to 10 cm in front of the nose with a width between 2 cm and 2.5 cm (~50 cm^3 in volume). In plane BP (Figure 12 a) differences along the X^B axis between the cases with and without gravity, are less than 0.1 mm. In MP (Figure 12 b) along Y^B axis there is a small difference (around 3 mm) between the delimitation of the zone with and without gravity. The zones thus delimited could be considered identical with and without gravity. Despite the thermal plume's influence on the breathing flow in the presence of gravity being evidenced in Chapter 4.1, it appears the FFT analysis is less sensitive to this effect. In Figure 12 a, b the BZ corresponds to higher velocity regions (>0.3 m/s) than caused by the human body thermal plume (0.25 m/s maximum), explaining why the BZ is the same with and without gravity. In Figure 12 c, the BZ is visible along with the axial changes of W^B_{max}, considering: one averaged cycle, the peak exhalation, and the peak inhalation fields. The averaged cycle's profile confirms that the mean velocity contour of 0.3 m/s, coincides with the border of the BZ (Figure 12 a and b) where W^B_{max} is 1 m/s at peak exhalation and 0 m/s at peak inhalation. In Figure 12 d, the BZ obtained by the FFT study is compared to the definitions proposed by Haselton [19] and Hweij [32]. The 1 cm radius sphere of Hweij [32] is entirely contained within our BZ. The region of air that is rebreathed, according to Haselton [19], is also circumscribed in our BZ. The inhalation hemisphere designated by Haselton [19] (radius 6.2 cm) is visible in Figure 12 d and is probably relevant at peak inhalation, but does not include all the states of breathing flow over the entire inhalation half-cycle as the authors do in this study.

To directly link the identified BZ to the accumulation of CO_2, we have superposed in Figure 12 e, f the BZ and the ΔCO_2 distributions, comparing the peak exhalation (Figure 12 e) with the peak inhalation (Figure 12 f). At peak exhalation, the BZ is located in the region where ΔCO_2 is equal to 0 indicating no difference in CO_2 concentration between the two cases. At peak inhalation, the BZ is located in a region of positive ΔCO_2. To the extent that the BZ obtained is relevant, this means that the air inhaled by the astronaut is charged with more CO_2 in comparison to a similar situation on Earth.

(a) **(b)**

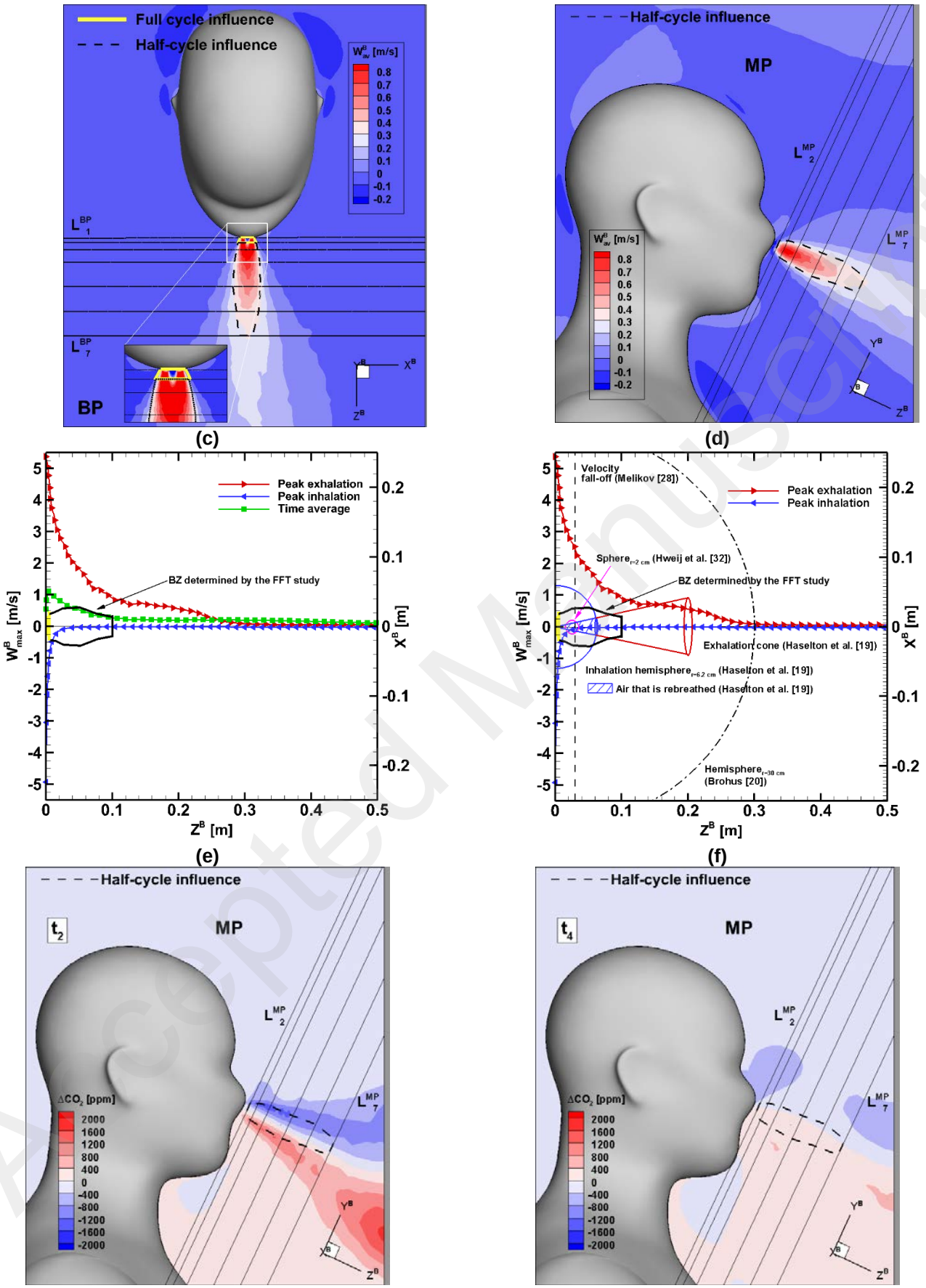

Figure 12 Zones influenced by the breathing cycle in planes MP (a) and BP (b). BZ determined by the FFT analysis superposed on W^B_{max} plots (c) with other BZ definitions (d); ΔCO_2 contours superposed on the BZ at instants t_2 (e) and t_4 (f).

5. Conclusions

The spatial distribution of breath CO_2 in the CQ of the ISS has been evaluated numerically, in order to circumscribe the region needing ventilation to prevent the astronaut's intoxication during sleep. This result required a multi-step approach.

Lacking CO_2 accumulation data inside the CQ in microgravity, a coupled experimental and numerical simulation of the accumulation problem was necessary on Earth, in order to obtain a valid model.

Experimental measurements performed with human subjects in the confined environment of a full-scale CQ mock-up, provided the CO_2 accumulation at different locations. A numerical model reproducing the experimental setup with a human model placed inside, aimed to replicate the CO_2 accumulation observed experimentally, using a realistic breathing function with gravity. The numerical results are in general accord with the experimental results.

The same numerical model was run again without gravity and compared to the one with gravity, directly investigating the difference ΔCO_2 between the distribution of CO_2 concentration with and without gravity. Positive values of ΔCO_2 were correlated to the trajectory of the breath's flow (high velocities). Negative values were associated with low velocity zones, where buoyancy plays a role in the airflow, when gravitational acceleration is present. High accumulations of CO_2 were found in the region in front of the astronaut's face.

The respiratory flow was analyzed in terms of overall behavior, comparable to twin jets at peak exhalation, and in dynamically looking for a rigorous definition of the BZ. The far field twin jets expansion was found to be close to previously reported values in the case of mouth breathing flow. For a more rigorous delimitation of the BZ, the zone influenced by the breath was spatially delimited by applying FFTs to the breath flow velocity variation over time along multiple lines in front of the human head. This FFT analysis delineated a small region influenced by the full breathing cycle, followed by a larger region presenting the influence of a half breathing cycle. The latter coincides with the high velocity region of the mean breathing velocity field (> 0.3 m/s). The BZ remained unchanged with or without gravity following this method. The resulting BZ encompassed two other BZ definitions, whose spatial limitation is not explained in the literature.

Finally, a direct link was made between the BZ and ΔCO_2 distribution. Without gravity, the air inhaled by the astronaut is charged with more CO_2 in comparison to a similar situation on Earth. A personalized ventilation system can be introduced in addition to the general one, targeted on the resulting BZ, to supply air less concentrated in CO_2 where it is needed. Future research will build upon the current results and investigate the viability of integrating a personalized ventilation system for the astronaut's CQ.

Acknowledgements

This work was supported by a "Presidency" scholarship from the University of Rennes 1, for which the authors are grateful.

This work was also supported by the grant of the Romanian Space Agency ROSA STAR-CDI-C3-2016-577.

REFERENCES

[1] NASA, National Aeronautics and Space Administration HUMAN INTEGRATION DESIGN HANDBOOK, Spaceflight (Lond). (2010) 1–27. https://doi.org/NASA/SP-2010-3407.

[2] R.M. Bagdigian, N. Marshall, S. Flight, International Space Station Environmental Control and Life Support System Mass and Crewtime Utilization In Comparison to a Long Duration Human Space Exploration Mission, (2015).

[3] C.M. Matty, Overview of Carbon Dioxide Control Issues During International Space Station/Space Shuttle Joint Docked Operations, 40th Int. Conf. Environ. Syst. 2 (2010) 1–9. https://doi.org/10.2514/6.2010-6251.

[4] F. Shiming, P. Yifei, Influence of IMV on Space Station, Eng. Technol. (2009) 831–835.

[5] S. Fairburn, S. Walker, 'Sleeping With the Stars' – The Design of a Personal Crew Quarter for the International Space Station, in: 31st Int. Conf. Environ. Syst., 2001. https://doi.org/10.4271/2001-01-2169.

[6] J.T. James, The headache of carbon dioxide exposures, SAE Tech. Pap. (2007). https://doi.org/10.4271/2007-01-3218.

[7] T.P. Schlesinger, B.R. Rodriguez, International Space Station Crew Quarters On-Orbit Performance and Sustaining Activities, Int. Conf. Environ. Syst. (2013) 1–9. https://doi.org/10.2514/6.2013-3515.

[8] EUROPEAN COMMITTEE FOR STANDARDIZATION, En 13779, Management. (2007) 72.

[9] J.T. James, V.E. Meyers, W. Sipes, R.R. Scully, C.M. Matty, Crew Health and Performance Improvements with Reduced Carbon Dioxide Levels and the Resource Impact to Accomplish Those Reductions, (2011) 1–7.

[10] D. Law J., Watkins S., Alexander, W.S. Law J., In-Flight Carbon Dioxide Exposures and Related Symptoms: Associations, Susceptibility and Operational Implications, NASA Tech. Rep. (2010) 1–21. https://doi.org/NASA/TP-2010-216126.

[11] C.H. Son, E.M. Smirnov, N.G. Ivanov, D.S. Telnov, Cfd Modeling of International Space Station and Visiting Spacecraft Ventilation : Evaluation of Design Solutions for Complex on-Orbit Operations, 3 (2011).

[12] C. Son, J. Zapata, C. Lin, Investigation of Airflow and Accumulation of Carbon Dioxide in the Service Module Crew Quarters, Int. Conf. Environ. Syst. (2002) 2341. https://doi.org/10.4271/2002-01-2341.

[13] C. Son, N. Ivanov, D. Telnov, E. Smirnov, Integrated Ventilation Modeling for Crew Quarter Airflow, 41st Int. Conf. Environ. Syst. (2011). https://doi.org/doi:10.2514/6.2011-5079.

[14] C.H. Son, N.G. Ivanov, E.M. Smirnov, D.S. Telnov, CFD analysis of node 1 ventilation and carbon dioxide transport for the maximum stowage configuration, 40th Int. Conf. Environ. Syst. ICES 2010. (2010) 1–9. https://www.scopus.com/inward/record.uri?eid=2-s2.0-84880815509&partnerID=40&md5=90d65d3b6de73053631251129e08198a.

[15] C.H. Son, Computational Fluid Dynamics Ventilation Study for the Human Powered Centrifuge at the International Space Station, (2012) 1–9. https://stitest-ntrs.larc.nasa.gov/search.jsp?R=20120010530.

[16] E.M. Smirnov, N.G. Ivanov, D.S. Telnov, C.H. Son, CFD modelling of cabin air ventilation in the international space station: A comparison of RANS and LES data with test measurements for the Columbus module, Int. J. Vent. 5 (2006) 219–227. https://doi.org/10.1080/14733315.2006.11683739.

[17] S. Mazumdar, Q. Chen, Influence of cabin conditions on placement and response of contaminant detection sensors in a commercial aircraft, J. Environ. Monit. 10 (2008) 71–81. https://doi.org/10.1039/b713187a.

[18] T. Zhang, Q. Chen, Identification of contaminant sources in enclosed spaces by a single sensor, Indoor Air. 17 (2007) 439–449. https://doi.org/10.1111/j.1600-0668.2007.00489.x.

[19] F.R. Haselton, P.G.N. Sperandio, Convective exchange between the nose and the atmosphere, J. Appl. Physiol. 64 (1988) 2575–2581. https://doi.org/10.1152/jappl.1988.64.6.2575.

[20] H. Brohus, Measurement of Personal Exposure Using a Breathing Thermal Manikin, Aalborg Univ. (1997).

[21] S.R. Dinardi, The Occupational Environment: Its Evaluation and Control and Management, 1997.

[22] Council of the European Union, EN 15251 CEN/TC 156 Indoor environmental input parameters for design and assessment of energy performance of buildings- addressing indoor air quality, thermal environment, lighting and acoustics, (2006) 1–52.

[23] U.S. Department of Energy, DOE-HDBK-1188-2006 Glossary of Environment, Safety and Health Terms, (2006) 158.

[24] EUROPEAN COMMITTEE FOR STANDARDIZATION, EN ISO 18158:2016, 2016.

[25] A.K. Melikov, R. Cermak, M. Majer, Personalized ventilation: Evaluation of different air terminal devices, Energy Build. 34 (2002) 829–836. https://doi.org/10.1016/S0378-7788(02)00102-0.

[26] G. Lidén, J. Surakka, A headset-mounted mini sampler for measuring exposure to welding aerosol in the breathing zone, Ann. Occup. Hyg. 53 (2009) 99–116. https://doi.org/10.1093/annhyg/mep001.

[27] J. Pantelic, S. Liu, L. Pistore, D. Licina, M. Vannucci, S. Sadrizadeh, A. Ghahramani, B. Gilligan, E. Sternberg, K. Kampschroer, S. Schiavon, Personal CO2 cloud: laboratory measurements of metabolic CO2 inhalation zone concentration and dispersion in a typical office desk setting, J. Expo. Sci. Environ. Epidemiol. 30 (2020) 328–337. https://doi.org/10.1038/s41370-019-0179-5.

[28] A.K. Melikov, Personalized Ventilation, Indoor Air. 14 (2004) S541–S549. https://doi.org/10.3233/THC-161180.

[29] D. Rim, A. Novoselec, G. Morrison, The influence of chemical interactions at the human surface on breathing zone levels of reactants and products, Indoor Air. 19 (2009) 324–334. https://doi.org/10.1111/j.1600-0668.2009.00595.x.

[30] D.R. Marr, I.M. Spitzer, M.N. Glauser, Anisotropy in the breathing zone of a thermal manikin, Exp. Fluids. 44 (2008) 661–673. https://doi.org/10.1007/s00348-007-0425-9.

[31] C. Chen, R. You, Differentiating between direct and indirect exposure to exhaled particles in indoor environments with mechanical ventilation systems, E3S Web Conf. 111 (2019). https://doi.org/10.1051/e3sconf/201911104034.

[32] W. Abou Hweij, N. Ghaddar, K. Ghali, C. Habchi, Optimized performance of displacement ventilation aided with chair fans for comfort and indoor air quality, Energy Build. 127 (2016) 907–919. https://doi.org/10.1016/j.enbuild.2016.06.052.

[33] D. Al Assaad, K. Ghali, N. Ghaddar, C. Habchi, Mixing ventilation coupled with personalized sinusoidal ventilation: Optimal frequency and flow rate for acceptable air quality, Energy Build. 154 (2017) 569–580. https://doi.org/10.1016/j.enbuild.2017.08.090.

[34] D. Al Assaad, C. Habchi, K. Ghali, N. Ghaddar, Effectiveness of intermittent personalized ventilation in protecting occupant from indoor particles, Build. Environ. 128 (2018) 22–32. https://doi.org/10.1016/j.buildenv.2017.11.027.

[35] E. Katramiz, D. Al Assaad, N. Ghaddar, K. Ghali, The effect of human breathing on the effectiveness of intermittent personalized ventilation coupled with mixing ventilation, Build. Environ. 174 (2020) 106755. https://doi.org/10.1016/j.buildenv.2020.106755.

[36] J.L. Broyan, M.A. Borrego, J.F. Bahr, International Space Station USOS Crew Quarters Development, 38th Int. Confeence Environ. Syst. (2008). https://doi.org/10.4271/2008-01-2026.

[37] J. Broyan, D. Welsh, S. Cady, International Space Station Crew Quarters Ventilation and Acoustic Design Implementation, 40th Int. Conf. Environ. Syst. (2010) 1–16. https://doi.org/10.2514/6.2010-6018.

[38] EN ISO, 14505-3, 2006.

[39] F. Bode, A. Meslem, C. Patrascu, I. Nastase, Flow and wall shear rate analysis for a cruciform jet impacting on a plate at short distance, Prog. Comput. Fluid Dyn. 20 (2020) 169–185. https://doi.org/10.1504/PCFD.2020.107276.

[40] J.K. Gupta, C.H. Lin, Q. Chen, Characterizing exhaled airflow from breathing and talking, Indoor Air. 20 (2010) 31–39. https://doi.org/10.1111/j.1600-0668.2009.00623.x.

[41] P.. John E. Hall, Guyton and Hall Textbook of Medical Physiology 12th Ed [PDF][tahir99] VRG, 12th ed., SAUNDERS Elsevier, 2011.

[42] I.D. O'Brien, E. Shacklock, A. Middleditch, C. Bigham, Inaccuracies in calculating predicted body weight and its impact on safe ventilator settings, J. Intensive Care Soc. 17 (2016) 191–195. https://doi.org/10.1177/1751143715626163.

[43] W.C. Adams, Measurement of Breathing Rate and Volume in Routinely Performed Daily Activities, Calif. Environ. Prot. Agency. 6 (1993) S30. https://doi.org/10.1097/00001648-199503000-00162.

[44] E. Bjørn, P. V. Nielsen, Dispersal of exhaled air and personal exposure in displacement ventilated rooms, Indoor Air. 12 (2002) 147–164. https://doi.org/10.1034/j.1600-0668.2002.08126.x.

[45] H. Qian, Y. Li, P. V. Nielsen, C.E. Hyldgaard, T.W. Wong, A.T.Y. Chwang, Dispersion of exhaled droplet nuclei in a two-bed hospital ward with three different ventilation systems, Indoor Air. 16 (2006) 111–128. https://doi.org/10.1111/j.1600-0668.2005.00407.x.

[46] I. Olmedo, P. V. Nielsen, M. Ruiz de Adana, R.L. Jensen, P. Grzelecki, Distribution of exhaled contaminants and personal exposure in a room using three different air distribution strategies, Indoor Air. 22 (2012) 64–76. https://doi.org/10.1111/j.1600-0668.2011.00736.x.

[47] I. Olmedo, P. V. Nielsen, M.R. de Adana, R.L. Jensen, The risk of airborne cross-infection in a room with vertical low-velocity ventilation, Indoor Air. 23 (2013) 62–73. https://doi.org/10.1111/j.1600-0668.2012.00794.x.

[48] G. Cao, P. V. Nielsen, R.L. Jensen, P. Heiselberg, L. Liu, J. Heikkinen, Protected zone ventilation and reduced

personal exposure to airborne cross-infection, Indoor Air. 25 (2015) 307–319. https://doi.org/10.1111/ina.12142.

[49] L. Liu, Y. Li, P. V. Nielsen, J. Wei, R.L. Jensen, Short-range airborne transmission of expiratory droplets between two people, Indoor Air. 27 (2017) 452–462. https://doi.org/10.1111/ina.12314.

[50] S.J. Yoo, K. Ito, Assessment of transient inhalation exposure using in silico human model integrated with PBPK-CFD hybrid analysis, Sustain. Cities Soc. 40 (2018) 317–325. https://doi.org/10.1016/j.scs.2018.04.023.

[51] F.A. Berlanga, L. Liu, P. V. Nielsen, R.L. Jensen, A. Costa, I. Olmedo, M.R. de Adana, Influence of the geometry of the airways on the characterization of exhalation flows. Comparison between two different airway complexity levels performing two different breathing functions, Sustain. Cities Soc. 53 (2020) 101874. https://doi.org/10.1016/j.scs.2019.101874.

[52] Z. Cheng, C. Guangyu, A. Aganovic, L. Baizhan, Experimental study of the interaction between thermal plumes and human breathing in an undisturbed indoor environment, Energy Build. 207 (2020) 109587. https://doi.org/10.1016/j.enbuild.2019.109587.

[53] C. Xu, P. V. Nielsen, G. Gong, L. Liu, R.L. Jensen, Measuring the exhaled breath of a manikin and human subjects, Indoor Air. 25 (2015) 188–197. https://doi.org/10.1111/ina.12129.

[54] T. Zhang, S. Yin, S. Wang, Quantify impacted scope of human expired air under different head postures and varying exhalation rates, Build. Environ. 46 (2011) 1928–1936. https://doi.org/10.1016/j.buildenv.2011.03.014.

[55] 1994 ASHRAE Handbook - Fundamentals, 1994.

[56] H. Awbi, Ventilation of Buildings, 2nd ed., 2003.

[57] S. Yao, C. Min, H. Ye, Q. Fu, Y. Duan, L. Feng, N. Jiang, H. Sun, J. Liu, Experimental study on flow behavior of breathing activity produced by a thermal manikin, Build. Environ. 123 (2017) 200–210. https://doi.org/10.1016/j.buildenv.2017.07.004.